Optics Letters

Two-stage artificial neural network-based burst-subcarrier joint equalization in nonlinear frequency division multiplexing systems

Xinyu Chen,[1] Hao Ming,[1] Chenjia Li,[1] Guangqiang He,[2] and Fan Zhang[1,*]

[1]State Key Laboratory of Advanced Optical Communication Systems and Networks, Frontiers Science Center for Nano-optoelectronics, Department of Electronics, Peking University, Beijing 100871, China
[2]State Key Laboratory of Advanced Optical Communication Systems and Networks, Department of Electrical Engineering, Shanghai Jiao Tong University, Shanghai 200240, China
*Corresponding author: fzhang@pku.edu.cn

Received 10 February 2021; accepted 23 February 2021; posted 3 March 2021 (Doc. ID 422195); published 25 March 2021

We propose an artificial neural network (ANN)-based scheme to improve the performance of nonlinear frequency division multiplexing (NFDM) optical transmission systems in both time and frequency domain. Through two-stage ANN equalization at the receiver side, time-domain distortions between adjacent bursts and frequency-domain cross talk between neighboring subcarriers can be jointly mitigated. Burst ANN and Subcarrier ANN equalizers are characterized and validated by numerical simulations of a dual-polarization NFDM transmission system. Compared with the basic detection scheme, the proposed two-stage ANN achieves a Q-factor gain of 3.01 dB for an NFDM system with 256 Gb/s gross data rate transmitting over 960 km standard single-mode fiber (SSMF). The two-stage ANN approach offers an effective way to jointly equalize the signal in multiple dimensions.

https://doi.org/10.1364/OL.422195

Over the past years, a revolutionary transmission scheme called nonlinear frequency division multiplexing (NFDM) has been actively investigated to treat fiber nonlinearity as a constructive effect, rather than a destructive feature [1]. This approach uses nonlinear Fourier transform (NFT) [2] against Kerr nonlinear damage with data modulated on the nonlinear spectrum (NS) that evolves linearly in the fiber channel. As two elements of the NS, discrete spectrum (DS, soliton spectral components) and continuous spectrum (CS, dispersive waves) can both be utilized as information media [3]. In principle, the interplay between nonlinearity and dispersion can be eliminated with a single-tap equalizer at the receiver [3], which can reverse the channel impact in nonlinear Fourier domain. Nevertheless, many technical problems with the NFDM schemes are still ongoing before NFDM systems become practical and outperform conventional systems [4–6].

Considering the realistic channel, existing inevitable noise breaks down the independence of the subcarriers in the nonlinear frequency domain [6]. The interference tends to be more complicated because of the signal temporal dispersive spreading [4,7] and the noise contained in the NFT computation window [8]. Various detection strategies based on nonlinear spectral noise analysis were implemented to improve the performance, revealing great potential superior to original NFDM systems [9,10]. Although nonlinear spectral noise properties have been widely investigated [4,8], it is still ambiguous to utilize the stochastic characteristics of noise in the nonlinear domain for designing the optimum receiver. Therefore, several novel techniques based on machine learning (ML) have been proposed [11–13], for the superiority of ML in figuring out the influence of noise and cutting down the extent of its perturbation. In particular, a supervised ML technique was developed for the CS of a single polarization NFDM system [14], which mitigated the negative impacts through spectral equalization. The successful applications of ML call for more approaches that can consider distortions in multiple dimensions.

In this Letter, we propose a two-stage equalization scheme based on artificial neural network (ANN) in NFDM systems with CS modulation. A Burst ANN equalizer and a Subcarrier ANN equalizer are designed at the receiver side to enhance the performance of the NFT-based optical transmission system. The pronounced performance improvement is achieved with the joint ANN equalizers.

The standard single-mode fiber (SSMF) supports two orthogonal polarization components for high spectral efficiency optical transmission. The normalized complex envelope $\mathbf{q}$ of dual-polarization (DP) optical signal propagation along an ideal, noiseless optical fiber is characterized as Eq. (1) [15]. Here, normalized variables l and t, respectively, denote the location in the fiber and the retarded time,

$$\frac{\partial \mathbf{q}}{\partial l} + j\frac{\partial^2 \mathbf{q}}{\partial t^2} + 2j\|\mathbf{q}\|^2\mathbf{q} = 0. \tag{1}$$

The DP-NFDM system is simulated with commercial software VPItransmissionMaker 9.5 as diagrammed in Fig. 1. The system parameters are listed in Table 1. The $L = 960$ km fiber link consists of $N_{\text{span}} = 12$ spans. In each span of $L_{\text{span}} = 80$ km, fiber attenuation is compensated by an erbium-doped fiber amplifier (EDFA).

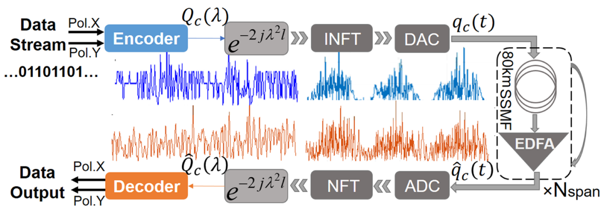

Fig. 1. Diagram of the DP-NFDM system.

The transmitted CS $Q_c(\lambda)$ comes into being via a similar manner of orthogonal frequency-division multiplexing (OFDM) modulation with N_C subcarriers as Eq. (2),

$$Q_{c(i)}(\lambda) = \sum_{k=-Nc/2}^{Nc/2} m_{k(i)} \frac{\sin(\lambda T_0 + k\pi)}{\lambda T_0 + k\pi}, \quad i = 1, 2. \quad \textbf{(2)}$$

Here $m_{k(i)}$ is the symbol of 16-ary quadrature-amplitude modulation (16-QAM). $i = 1, 2$ represents polarization x and y, respectively; λ is the nonlinear frequency; and T_0 is the useful time duration. To fulfill the vanishing boundary conditions of NFT, the transmission is organized in bursts separated in time, as shown by $q_c(t)$ in Fig. 1. The guard interval (GI) between bursts should also account for temporal broadening caused by chromatic dispersion to avoid inter-symbol interference. With pre-dispersion compensation (PDC) ($e^{-2j\lambda^2 l}$ phase rotation of transmitted nonlinear spectra) [16], the least required interval time T_G is derived from channel memory estimated as $T_G \geq \pi W \beta_2 L$ [17]. The GI factor is defined as $g = (T_0 + T_G)/T_0$ [18]. With T_0 fixed, a larger g stands for longer GI but leads to a lower proportion of effective information. A proper g is a trade-off between the system performance and spectral efficiency.

The properties of an NFT-based communication system are affected by the interplay between the link noise and the computation noise [8], which leads to disturbances appeared in both time and frequency domains. Hence, we propose a burst-subcarrier joint equalization to redeem deficient performance. To obtain baseline characteristics of the DP-NFDM system, we adopt q-modulation and the conventional detection scheme as [18]. To benchmark the achievable enhancement by ANN, we also use a phase equalization method with the aided pilots [19], which contributes to removing common phase noise in the frequency domain. The transmitter (Tx) side digital signal processing (DSP) is displayed in Fig. 2(a), while the receiver (Rx) side DSP flows of our proposed method and the pilot-assisted equalization are shown in Fig. 2(b). The conventional detection scheme is displayed in Fig. 2(b) by excluding the yellow modules that correspond to the pilot and the ANN scheme. Note that the conventional scheme is a single-tap channel equalization to remove the accumulated phase rotation retrieving the data-bearing CS.

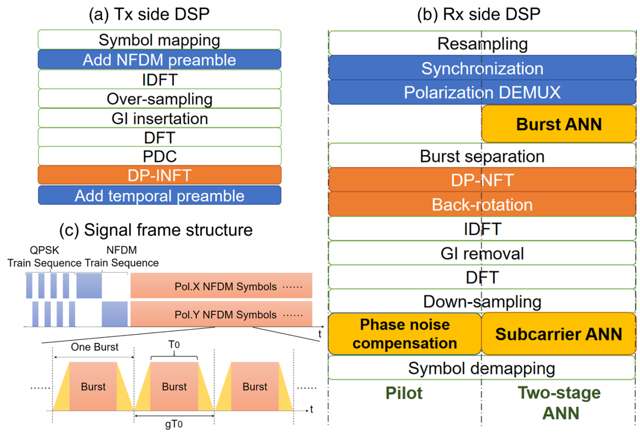

Fig. 2. (a) Tx side DSP, (b) Rx side DSP. (c) Signal structure in simulation.

The frame structure is shown in Fig. 2(c), which consists of the training sequences and the NFDM symbol bursts for data carrying. Pairs of time-multiplexed training sequences are across the two polarizations [20], including quadrature phase shift keying (QPSK) symbols (for synchronization and polarization demultiplexing) and an NFDM burst (for removing signal amplitude scaling). The NFDM burst signals are processed with NFT and inverse NFT (INFT) algorithms, respectively, by the Boffetta–Osborne integration scheme and the Ablowitz–Ladik scheme [3]. For the system detailed in Table 1, the gross data rate is 256 Gb/s, while the net bit rate is determined with both frame redundancy (GI and training sequences) and the 7% hard-decision forward error correction (HD-FEC) overhead considered. The system performance is evaluated with the Q-factors of different equalization schemes at different launch power. The Q-factor is derived from the bit error rate (BER) by $Q^2_{\mathrm{dB}} = 20\log_{10}[\sqrt{2}\mathrm{erfc}^{-1}(2\mathrm{BER})]$ [21].

In the time domain, there exist burst corruptions induced by various factors within adjacent bursts. In the frequency domain, the physical distortion noise and the numerical noise destroy the independence of each subcarrier on which data symbols are modulated [13]. To overcome the correlation problems between the NS components, a multi-tap equalization of spectrum-based NN is recently proposed [14]. Whereas adverse correlations occur both in the time and frequency domains, we propose a two-stage ANN equalization scheme as depicted in Fig. 3. The burst equalization shown in Fig. 3(a) is performed temporally to process the received time-domain bursts. Burst samples are reshaped before being sent as inputs for the ANN. Owing to the boundary interference mostly occurring at the junction of the preceding burst and the following one, we reorganize temporal bursts into groups composed of three consecutive bursts. The intermediate burst of each group is the target to be equalized. The subcarrier equalization shown in Fig. 3(b) is performed after the phase rotation operation in NS. The input elements

Table 1. Parameters of the DP-NFDM System in the Simulation

Parameter	Value	Parameter	Value
Linear bandwidth (W)	32 GHz	Fiber attenuation (α)	0.2 dB/km
Center carrier frequency	193.1 THz	Fiber dispersion (β_2)	-21.5 ps^2/km
Span length (L_{span})	80 km	Fiber nonlinearity (γ)	1.3 W^{-1}/km^{-1}
Number of spans (N_{span})	12	EDFA noise figure (NF)	5 dB

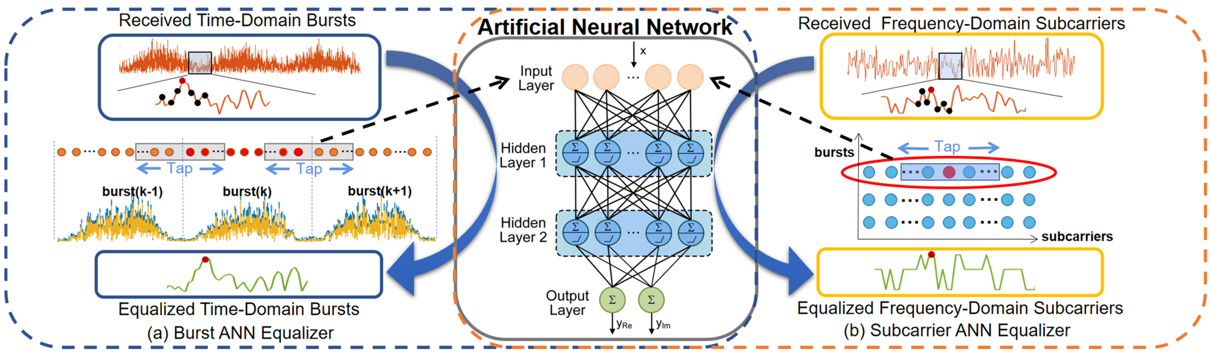

Fig. 3. Schematics of (a) burst equalizer and (b) subcarrier equalizer implemented as ANN. ANN inputs consist of a sample from received (a) time-domain bursts (red dot on the waveform) or (b) symbols on subcarriers (red dots on the subcarriers), and adjacent samples (black dots).

Table 2. Setups of the Neural Networks

		Number of Neurons				
Network	Activation Function	Input Layer (M)	Hidden Layer 1	Hidden Layer 2	Hidden Layer 3	Output Layer
Burst ANN	ReLU	82	21	11	None	2
Subcarrier ANN	ReLU	30	21	11	None	2
Spectrum-based NN [14]	Leaky RELU	42	64	64	64	2

of ANN are from the rotated spectrum of each burst. The Burst and the Subcarrier ANNs both act as multi-tap equalization and treat each polarization separately.

The ANNs used in two stages are sketched in the middle of Fig. 3, which have the same structure but different input layer sizes. The detailed setups of our proposed two-stage ANN are shown in Table 2 together with that of the spectrum-based NN [14] for a comparison. The network function y_{NL} of the ANN-based equalizer can be expressed as Eq. (3),

$$y_{\mathrm{NL}} = \mathbf{w}_3 \hat{f}\left(\mathbf{w}_2 \hat{f}\left(\mathbf{w}_1 \mathbf{x}_{B/C}\right)\right). \tag{3}$$

$\mathbf{x}_B$ denotes the received time samples in each burst, while $\mathbf{x}_C$ is of the symbol samples on the subcarriers. The ANN input size M is related to the taps consisting of the sample itself and the adjacent samples. $\mathbf{w}_1$, $\mathbf{w}_2$, and $\mathbf{w}_3$ are weight matrices of hidden layer 1, hidden layer 2, and the output layer, respectively. In the training phase, training labels are the transmitted time burst samples for Burst ANN and the transmitted subcarrier symbols for Subcarrier ANN. Weight matrices are optimized by minimizing mean squared error (MSE) loss with the backpropagation (BP) algorithm [22], indicating the optimum match between the network outputs and the given undistorted labels.

The random data bits are generated by Mersenne Twister function in MATLAB during training and testing. Data sets come from the received NFDM bursts, corresponding to 2.5×10^5 temporal signal samples and 5.1×10^4 frequency-domain symbols in each stage. 32% of the signal data are used for training, and the rest of the test set is used for evaluating the system performance.

To validate Burst ANN, we fix subcarrier numbers at 512 to ensure the same NFT operation accuracy, because NFT operation is needed subsequently to obtain the final performance. Since the redundant noise and boundary interferences in NFT windows are mitigated, Burst ANN contributes to enhancing the performance, as demonstrated in Fig. 4(a). It shows a Q-factor gain of 2.15 dB over the conventional equalization scheme and 1.10 dB over the pilot-aided method in the case of $g = 1.6$. Burst ANN acts better when $g = 1.4$, which leads to 2.26 dB gain over the conventional equalization scheme and 1.29 dB over the pilot-aided method. Considering the strong relationship between GI and burst interference, the behavior of Burst ANN versus g is shown by the solid lines in Fig. 4(b). The pilot-aided performance varies with g and reaches the optimal at $g = 1.6$, while Burst ANN brings out noticeable performance enhancement and makes the Q-factor relatively stable when $g > 1.4$. It indicates that Burst ANN enables shorter GI, which contributes to enhancing the spectral efficiency.

With more subcarriers utilized, the NFT processing window involves denser information, causing more correlations between the NS components. In Fig. 4(b), the red dashed line indicates that the pilot-aided performance drops with the increase of subcarrier numbers. The blue dashed line shows that the larger performance gain appears when more subcarriers are involved, which indicates Subcarrier ANN performs more effectively for the NFDM systems with larger subcarrier numbers. For instance, a detailed comparison is given in Fig. 4(c), which shows the performances of the 256- and 512-subcarrier NFDM systems at their optimum g values. Subcarrier ANN achieves respective Q-factor gains of 0.43 dB and 0.55 dB over the pilot-aided phase correction method at the optimum powers for 256 and 512 subcarriers. Moreover, as indicated by the orange curves in Fig. 4(c), the performance of the Subcarrier ANN is similar to that of the spectrum-based NN [14]. It can be inferred that these two spectral multi-tap equalizations deal with not only the common phase rotation but also the imperfection caused by nonlinear interference for each subcarrier.

Figure 4 has presented the respective capabilities of Burst ANN and Subcarrier ANN, including performance enhancement in the case of shorter GI and/or more modulated subcarriers. In order to pinpoint the stepwise and overall effects of the two-stage ANN equalizer, the performances of separate equalization (Burst ANN, Subcarrier ANN) and joint equalization (Burst-Subcarrier ANN) in the 512-subcarrier NFDM system at $g = 1.4$ are depicted in Fig. 5. In view of 3.6% training sequences and 7% HD-FEC overhead, the net bit rate is 165.0 Gb/s (= 256/1.4/1.036/1.07). When burst-subcarrier equalization is jointly applied, the Q-factor is further upgraded by 0.75 dB improvement over the Burst ANN only, which brings about 3.01 dB total Q-factor gain compared with the

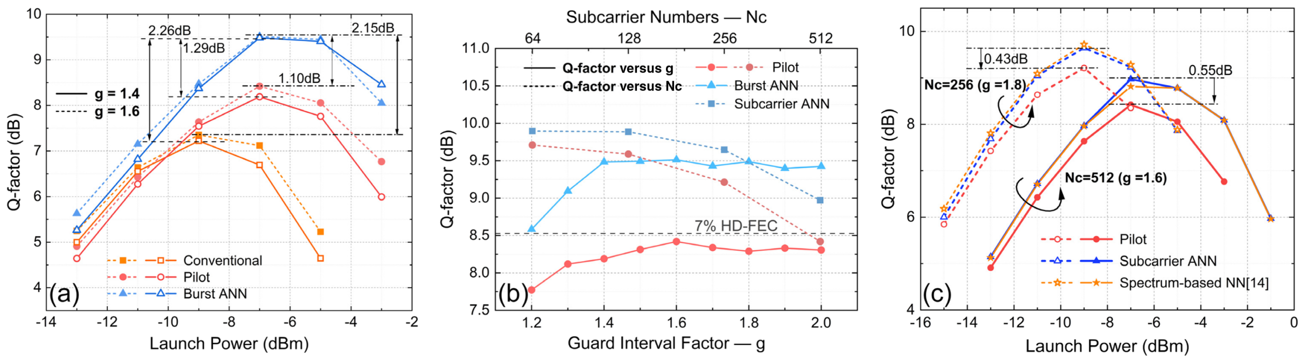

Fig. 4. (a) Performance of Burst ANN for $N_C = 512$; (b) Burst ANN performance versus g for $N_C = 512$ at optimum power -7 dBm (solid lines); Subcarrier ANN performance versus subcarrier numbers at each optimum power (dash lines); the proper g of 64-, 128-, 256-, and 512-subcarrier systems are, respectively, set at 2.6, 2.2, 1.8, and 1.6. (c) Performance of Subcarrier ANN.

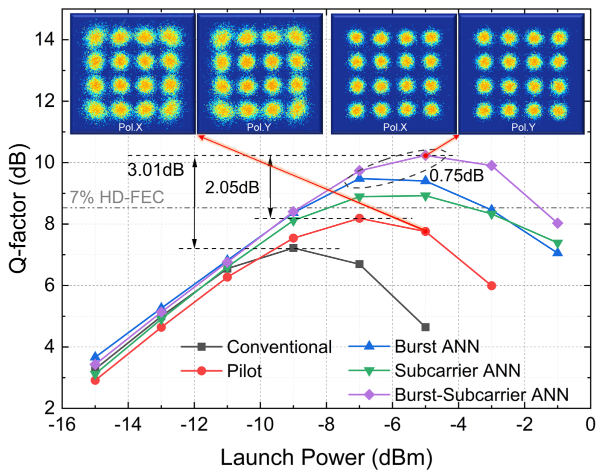

Fig. 5. Q-factor dependence on signal launch power over 960 km for $W = 32$ GHz, $N_C = 512$, $g = 1.4$. The constellations in the considered system with or without ANN at optimal power -5 dBm are plotted.

performance of the conventional equalization scheme. The optimal launch power is -5 dBm, which is 2.0 dB larger than that of the pilot-aided curve (Q-factor gain of 2.05 dB).

ANN brings performance gain while increasing calculation complexity. For the testing process, the multiplication numbers required for Burst ANN and Subcarrier ANN to equalize a sample are 1975 and 883 per polarization, respectively, as follows from Table 2.

In conclusion, the two-stage ANN equalizer is proposed to effectively compensate for both temporal and spectral impairments in nonlinear CS modulation. The simulation proves that this joint method can achieve about 3.01 dB Q-factor improvement for an NFDM system with 165.0 Gb/s net bit rate transmitting over 960 km SSMF. We note that the proposed equalizer is useful for eliminating adverse correlation between independent components of NFDM signals. The Burst ANN yields higher tolerance for shorter GI and noise, while the Subcarrier ANN enables longer burst length. The utilization of ANN specifically targets the physical distortions in multiple dimensions, which results in great superiority over the conventional and the pilot-assisted equalization scheme. We believe that such an ANN assisted methodology plays a promising role in signal equalization and detection in NFDM systems.

Funding. National Key Research and Development Program of China (2018YFB1801204); National Natural Science Foundation of China (61911530162, 62075129).

Disclosures. The authors declare no conflicts of interest.

REFERENCES

1. S. K. Turitsyn, J. E. Prilepsky, S. T. Le, S. Wahls, L. L. Frumin, M. Kamalian, and S. A. Derevyanko, Optica **4**, 307 (2017).
2. M. J. Ablowitz, B. Prinari, and A. D. Trubatch, *Discrete and Continuous Nonlinear Schroedinger Systems* (Cambridge University Press, 2004).
3. M. Yousefi and F. Kschischang, IEEE Trans. Inf. Theory **60**, 4312 (2014).
4. S. Civelli, E. Forestieri, and M. Secondini, IEEE Photon. Technol. Lett. **29**, 1332 (2017).
5. I. T. Lima, T. D. DeMenezes, V. Grigoryan, M. O'Sullivan, and C. R. Menyuk, J. Lightwave Technol. **35**, 5056 (2017).
6. X. Yangzhang, D. Lavery, P. Bayvel, and M. Yousefi, J. Lightwave Technol. **36**, 485 (2018).
7. S. A. Derevyanko, J. E. Prilepsky, and S. K. Turitsyn, Nat. Commun. **7**, 12710 (2016).
8. M. Pankratova, A. Vasylchenkova, S. A. Derevyanko, N. B. Chichkov, and J. E. Prilepsky, Phys. Rev. Appl. **13**, 054021 (2020).
9. S. Civelli, E. Forestieri, and M. Secondini, Opt. Express **26**, 12057 (2018).
10. T. Gui, T. H. Chan, C. Lu, A. P. T. Lau, and P.-K. A. Wai, J. Lightwave Technol. **35**, 1542 (2017).
11. S. Gaiarin, R. T. Jones, D. R. Francesco, and D. Zibar, *Conference on Lasers and Electro-Optics Europe (CLEO)* (2020), paper SF2L.4.
12. S. Gaiarin, F. Da Ros, N. D. Renzis, R. T. Jones, and D. Zibar, J. Lightwave Technol. **38**, 6465 (2020).
13. O. Kotlyar, M. Pankratova, M. Kamalian, A. Vasylchenkova, J. E. Prilepsky, and S. K. Turitsyn, *IEEE British and Irish Conference on Optics and Photonics (BICOP)* (2018), pp. 1–4.
14. O. Kotlyar, M. Pankratova, M. Kamalian, A. Vasylchenkova, J. E. Prilepsky, and S. K. Turitsyn, Opt. Lett. **45**, 3462 (2020).
15. S. V. Manakov, Sov. Phys. JETP **38**, 248 (1974).
16. S. T. Le, V. Aref, and H. Buelow, Nat. Photonics **11**, 570 (2017).
17. S. T. Le, V. Aref, and H. Buelow, J. Lightwave Technol. **36**, 1296 (2018).
18. X. Yangzhang, V. Aref, S. T. Le, H. Buelow, D. Lavery, and P. Bayvel, J. Lightwave Technol. **37**, 1570 (2019).
19. X. Yi, W. Shieh, and Y. Tang, IEEE Photon. Technol. Lett. **19**, 919 (2007).
20. X. Liu and F. Buchali, Opt. Express **16**, 21944 (2008).
21. I. P. Kaminow, T. Li, and A. E. Willner, *Optical Fiber Telecommunications V B: Systems and Networks* (Academic, 2008), Chap. 14.
22. D. E. Rumelhart, G. E. Hinton, and R. J. Williams, Nature **323**, 533 (1986).